J. of Supercritical Fluids 78 (2013) 7–11

Contents lists available at SciVerse ScienceDirect

The Journal of Supercritical Fluids

journal homepage: www.elsevier.com/locate/supflu

Molecular dynamics simulations of supercritical water at the iron hydroxide surface

Igor M. Svishchev*, Dimitrios T. Kallikragas, Andriy Yu. Plugatyr

Department of Chemistry, Trent University 1600 West Bank Drive, Peterborough, Ontario, Canada K9J 7B8

ARTICLE INFO

Article history:
Received 31 January 2013
Received in revised form 13 March 2013
Accepted 15 March 2013

Keywords:
Molecular dynamics
Supercritical water
Iron hydroxide

ABSTRACT

The adsorption properties of supercritical water confined between electrostatically neutral but hydrophilic surfaces of iron (II) hydroxide were determined through molecular dynamics simulations. Simulations were conducted at temperatures of 715, 814 and 913 K, and at water densities typically found in the heat transport system of the supercritical water cooled nuclear reactor (SCWR). Surface water layer densities were obtained and compared to those of the bulk water. Adsorption coverage was calculated as a function of the number of waters per OH group on the surface. Images of the water molecules configurations are provided along with the density profile of the adsorption layer. The localized adsorption and surface clustering of supercritical water, as seen in this study, would likely produce more localized corrosion phenomena in the water bearing components of the SCWR.

1. Introduction

Over the recent years much interest has been invested in the properties of high temperature and supercritical water. The thermodynamics, hydration and transport properties of aqueous systems at these conditions are of importance for a variety of applications, ranging from power generation to hazardous waste recycling and materials processing. [1–5]. Recently, molecular dynamics (MD) simulations have seen increased use in the study of the structure and dynamics of water at both mineral and metallic interfaces [6–8]. Molecular dynamics techniques have also been used in a variety of geophysical applications including carbon dioxide capture and sequestration, and in the investigation of intercalation in structural cavities and inter-layer spaces [9,10]. Supercritical water holds promise as the thermodynamically favorable medium of both neutron moderator and heat transfer fluid in the prospective GEN-IV supercritical water cooled nuclear reactor (SCWR). The lack of cavitation and high thermodynamic efficiency of the homogeneous supercritical phase provide the advantages of increased thermal efficiency and simpler design. The extreme corrosive properties of water in the supercritical state, is of particular concern in the physical design and choice of material for the heat exchange infrastructure. Much experimental work has been done in measuring the corrosion rates of different alloys and ceramic materials in an oxidative supercritical water environment. Thus far there is no one novel material capable of withstanding the corrosive properties of such an environment [11–17]. Stainless steel is one potential candidate for the supercritical water bearing components of the GEN-IV SCWR and it is prudent to understand the behavior of the $Fe(OH)_2$ hydroxide layer formed under these conditions. In order to minimize the corrosion in the heat transport systems of the currently deployed pressurized water reactors (PWRs), oxygen scavenging species such as hydrogen gas and hydrazine are added to the coolant, as well as lithium hydroxide for alkalinity control. The formation and accumulation of the hydroxide (and oxide) layer serves as a corrosion inhibiting surface that will protect the stainless steel from further oxidation, inhibiting more catastrophic corrosion such as stress corrosion cracking. To understand how such a layer forms, the adsorption characteristics of water must first be determined. Whether the water exhibits full or partial wetting will indicate if the corrosion is a general, surface wide phenomenon, or if rust will form in a more localized scenario, typical of pitting corrosion.

In this study, molecular dynamics simulations have been used as a means of overcoming the experimental challenges of the harsh supercritical water environment. Adsorption characteristics of supercritical water on the $Fe(OH)_2$ surface are presented for 715, 814 and 913 K at different water densities. Surface water layer densities were obtained and compared to those of the bulk water. An estimation of the adsorption kinetics for a low density system at 913 K is also included. The details of the simulations are presented in Section 2 and the results are presented in Section 3. Our conclusions are summarized in Section 4.

2. Simulation details

Classical molecular dynamics techniques were used to obtain the equations of motion via Lagrangian based methods [18]. The

* Corresponding author. Tel.: +1 705 748 1011x7063.
E-mail address: isvishchev@trentu.ca (I.M. Svishchev).

0896-8446/$ – see front matter © 2013 Elsevier B.V. All rights reserved.
http://dx.doi.org/10.1016/j.supflu.2013.03.016

simple point charge extended (SPC/E) model of water was used as it provides accurate thermodynamic properties over a wide range of temperatures and pressures, particularly at high temperatures. The equation of state (EOS) obtained from the SPC/E model is in good agreement with experimental results and so affords an accurate method, through the corresponding states principle, of investigating water systems at elevated temperatures and pressures [19,20]. The recently developed CLAYFF force field was used to obtain interaction parameters of the $Fe(OH)_2$ surfaces. CLAYFF has been used successfully to model the interaction energies of amorphous solids, oxides, layered hydroxides and interfacial systems [21,22]. Two electrostatically neutral $Fe(OH)_2$ surfaces were created by cleaving the equilibrated brucite crystal structure, at 298 K and 1 bar pressure, along the interlayer (0 0 1) plane and the OH groups were left intact. The simulation cell thus contained two crystalline slabs (comprised of two $Fe(OH)_2$ sheets each), consisting of a total of 162 Fe atoms and 324 OH groups per slab, with 81 OH groups (or equivalently, 81 unit cells of the brucite structure) on each side of the gap exposed to the water. The slabs had the dimensions of $29.3876 \times 25.4504 \times 9.208$ Å, with a 400 Å gap in between, with the overall simulation cell dimensions being, respectively, $29.3876 \times 25.4504 \times 418.416$ Å.

Table 1 shows the temperatures, total water densities and numbers of molecules in the simulations, along with the corresponding real water temperatures (as calculated using the EOS for the SPC/E water [19]). These state points mimic coolant conditions in the heat transport system of the SCWR. The water molecules were initially placed in a random configuration between the surfaces, and the system was allowed to equilibrate for the first 50 ps. The equations of motion were integrated using the Verlet algorithm with a 1 fs time step. An NVT ensemble was used and the temperature was maintained using the Nose-Hoover thermostat [23]. Periodic boundary conditions were employed and the atomic pair interactions were calculated using the Lorentz–Berthelot mixing rules, with a spherical cutoff radius set at half the (smallest side) cell length. Long-range Coulombic interactions were handled via the Ewald Summation method [18]. Intermediate averaging was performed every 1 ps and the simulations were allowed to proceed for a total time of 1 ns. The spacing of the surfaces remained constant throughout the simulations at about 400 Å, and no collapse of the crystalline blocks was detected.

Table 1
Parameters of simulated systems.

Temperature (K)	Corresponding real water temperature (K)	Total water density ($g\,cm^{-3}$)	$N(H_2O)$	$N(Fe)$	$N(OH)$
715	723	0.093	935	324	648
814	823	0.067	673	324	648
913	923	0.055	555	324	648
913	923	0.044	440	324	648

The simulations were performed on the Shared Hierarchy Academic Resource Computing Network (SHARCNET), a consortium of Ontario universities and colleges operating a network of high-performance computer clusters.

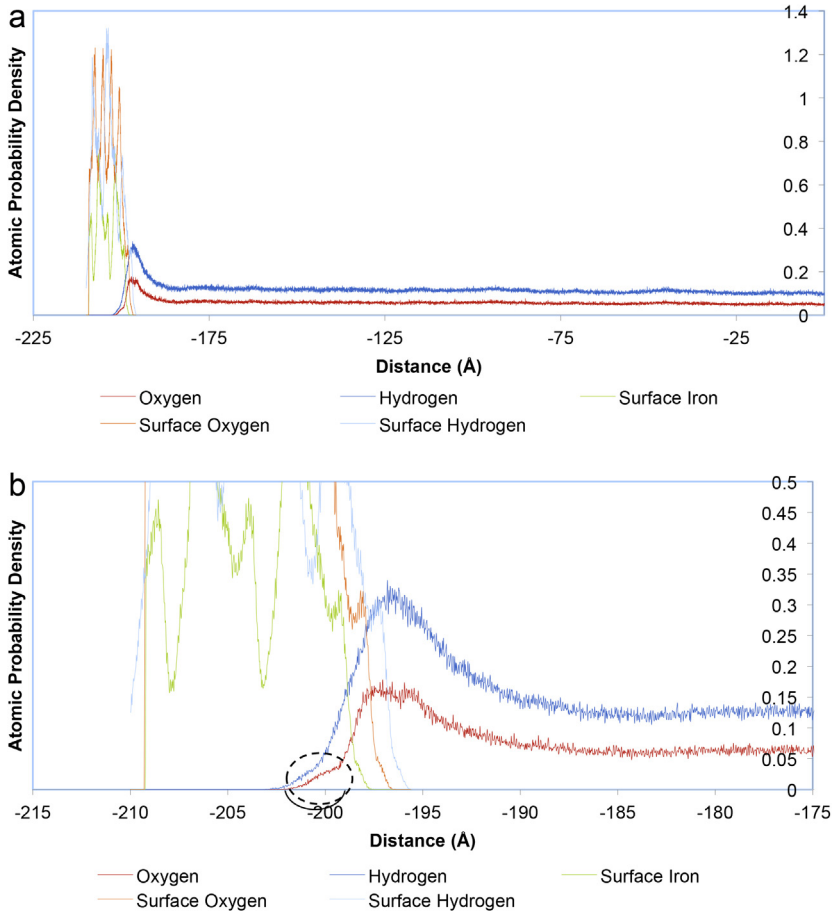

Fig. 1. (a) Atomic densities distribution at the supercritical water–iron (II) hydroxide interface at 715 K and total water density of 0.093 $g\,cm^{-3}$. The region shown is from the leftmost $Fe(OH)_2$ surface, to the center of the gap. Atomic density of the oxygen of the water molecule is shown in red, and hydrogen in blue. (b) Magnified view of the region at the left $Fe(OH)_2$ surface. The circle highlights the shoulder on density profiles due to adsorbed water penetrating further into the surface.

Table 2
Simulation results showing the bulk and surface water densities, number of adsorbed waters and Θ, the number of adsorbed waters per exposed OH group.

Temperature (K)	Bulk water density ($g\,cm^{-3}$)	Surface water density ($g\,cm^{-3}$)	Number of H_2O on surface	Θ
715	0.075	0.262	107	1.31
814	0.055	0.153	63	0.77
913	0.045	0.094	38	0.47
913	0.036	0.079	33	0.40

3. Results and discussion

The atomic density profile of the supercritical water–iron hydroxide interface for the 715 K system is shown in Fig. 1a, and an expanded view of the surface region is shown in Fig. 1b. The density profile shown represents the probability of finding a specific atom at a given distance in the direction normal to the surface, being computed as an average over the last 400 ps of the simulation trajectory. The region shown is from the plane at the left side of the gap at −210 Å to the center region at 0 Å. It can be seen from this density profile that the probability of water being present nearby the surface is substantially larger than in the bulk. Also evident from this figure, is that the majority of the water molecules at the surface are within the region up to outwards of about 185 Å from the origin, or 15 Å from the surface. The small shoulder in the water oxygen density profile (at all temperatures studied) at around ±200 Å suggests that a small number of adsorbed water molecules or roughly 10 percent (as determined from the integration of the density profile) penetrate further into the surface up to a distance of about 2 Å. The water dipoles in the nearest interfacial region are oriented outwards from the surface. Analysis of the peak positions at the maximums of the oxygen and hydrogen density profiles of the adsorbed water (Fig. 1), as well as at the maximums of the radial distribution functions between surface atoms and oxygen and hydrogen atoms of water molecules gives a most probable orientation of the dipoles of these interfacial waters. It appears to be approximately 50 degrees relative to the normal of the plane of the surface at the temperature of 715 K, decreasing to 35° at 913 K. Integration of the density profiles yielded the actual surface and bulk water densities as well as the actual number of water molecules found at the surface, and the results are shown in Table 2. To obtain the surface water density, the water oxygen density profile was integrated from the innermost edge of the surface at ±200 Å to the first minimum obtained from the 715 K isotherm which was found to be ±183.6 Å. This later value was also taken as the integration limit in the higher temperature simulations, due to the difficulty in resolving this minimum above 715 K. The bulk water density can be obtained by integrating the rest of the water oxygen distribution, i.e. from the minimum to the center of the cell. The number

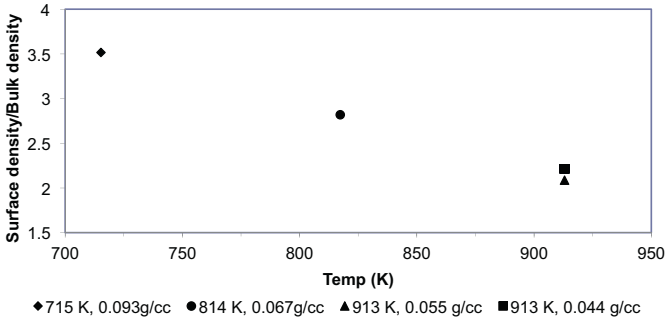

Fig. 2. Relative densities of the surface water layer with respect to the bulk water densities, at 715, 814, and 913 K. (For interpretation of the references to color in this figure legend, the reader is referred to the web version of the article.)

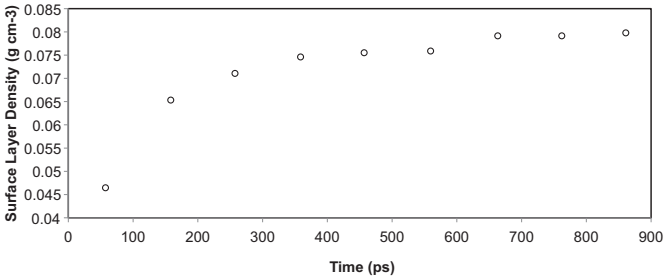

Fig. 3. Growth of the surface water layer over time at 913 K and total water density of 0.044 $g\,cm^{-3}$.

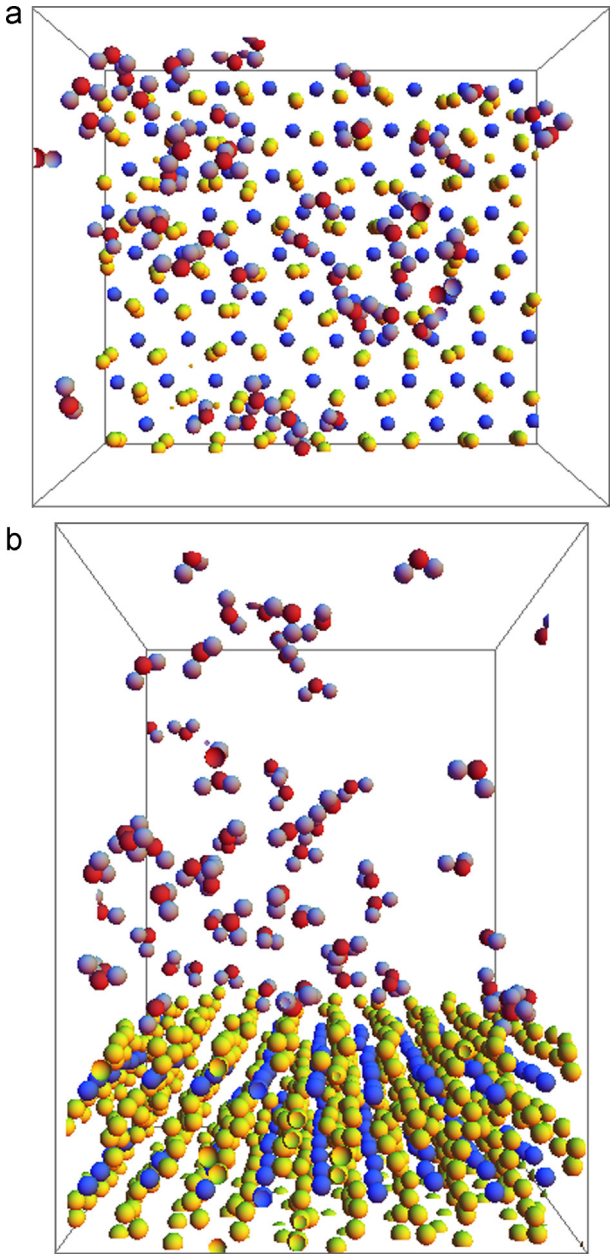

Fig. 4. Typical configurations of water molecules near the surface region at supercritical water conditions, at 715 K and total water density of 0.093 $g\,cm^{-3}$. Surface oxygens are shown in yellow and surface irons are shown in dark blue. The oxygens of the water are shown in red and the hydrogens in violet. (a) Top view and (b) side view. (For interpretation of the references to color in this figure legend, the reader is referred to the web version of the article.)

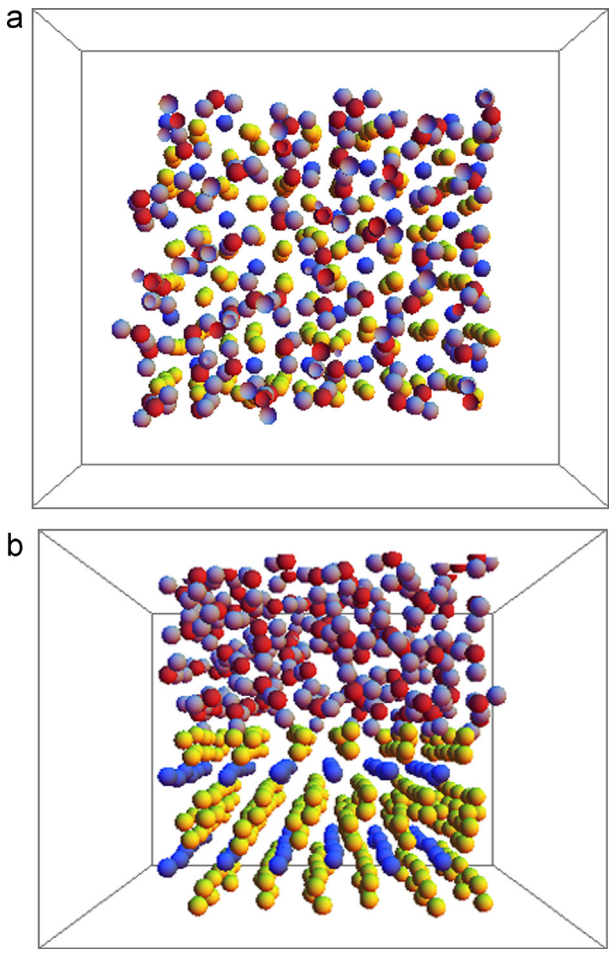

Fig. 5. Typical configurations of water molecules near the surface region at ambient conditions. Surface oxygens are shown in yellow and surface irons are shown in dark blue. The oxygens of the water are shown in red and the hydrogens in violet. (a) Top view and (b) side view. (For interpretation of the references to color in this figure legend, the reader is referred to the web version of the article.)

of adsorbed waters per exposed OH group, or the surface coverage, Θ, was seen to decrease with temperature and was at a maximum of 1.31 at 715 K and reached its lowest value of 0.40 for the 913 K system with the total water density of 0.044 g cm^{-3}. The relative density increase of the surface water layer with respect to the bulk was 3.5 at 715 K and decreased to 2.1 at 913 K for the system with the total water density of 0.055 g cm^{-3}. The results of the relative densities are plotted in Fig. 2.

We have performed an analysis of the growth of the surface water layer over time for the 913 K system and total water density of 0.044 g cm^{-3}. The surface layer density was calculated in block averages of 300 configuration step counts over intervals of 100 ps, starting with the initial total water density of 0.044 g cm^{-3} after 50 ps of equilibration time. The results are shown in Fig. 3. The analysis of the growth kinetics shows a logarithmic relationship between the density of the surface layer and time. Results indicate that the surface layer establishes itself quickly, with about 90 percent of the surface layer accumulating within the first 250 ps of simulation, with the density being relatively constant after the first half nanosecond.

Fig. 4 shows typical configurations of water molecules near the surface at supercritical water conditions (at 715 K and water density of 0.093 g cm^{-3}), while Fig. 5 displays interfacial structure at ambient conditions (at 298 K and water density of 1 g cm^{-3}). In Fig. 4(a) the top view of the atomic configuration shows a less uniform distribution of waters in contrast to the 298 K configuration in Fig. 5(a). The 715 K configuration shows more localized coordination of water with the adsorption occurring in small localized clusters. Figs. 4(b) and 5(b) show the side view of the 715 K and ambient systems, respectively. One can notice that in the supercritical system of 715 K and water density of 0.093 g m^{-3}, the surface layer is separated from the bulk with more waters being found near the surface and a low density region of small clusters being present outwards in the gap. To confirm these observations, we have inspected many configurations along the simulated trajectory. Instantaneous water structures look similar to those shown in Fig. 4 indicating a non-uniform coverage of the surface. Careful inspection of the generated configurations and atomic density profiles reveals that no permanent multi-layers are seen at the supercritical conditions studied as is often observed in subcritical surface systems [23]. As evident in Fig. 4, the supercritical water at the surface forms clusters with higher liquid like densities and regions of low density, gas like water. These results are consistent with the conclusions of Guzonas et al. [24], and can be explained by the tendency of water molecules to form small clusters, particularly near the ionic crystal surface, as the surface charges induce large density fluctuations that decay away from the surface. At supercritical conditions, when the dielectric constant of water and the density become small enough that they cannot sustain ion transport in the fluid, the gas phase chemical oxidation mechanism is thought to dominate in these low density water regions [24]. This would suggest that after the oxide/hydroxide layer is formed on the surface of the metal, the localized adsorption of the supercritical water would more likely lead to more localized pitting corrosion. On the other hand, it may accumulate in crevices of the surface leading to more serious, stress corrosion cracking in the water bearing components of the supercritical water cooled reactor.

4. Conclusions

The atomic density profile of the iron hydroxide–supercritical water system shows that the majority of the adsorbed water molecules are positioned within a few Angstroms, to about 15 Å, from the edge of the iron hydroxide surface. Their dipoles are generally oriented away from the surface. The density of water at the surface increases 2.2–3.5 times relative to bulk values depending on temperature and bulk water density. The surface water layer establishes itself quickly and reaches some 90 percent of its final density within the first 250 ps of simulation. From the images of water configurations, localized clustering is seen on the ionic surface at supercritical conditions, forming a higher (than bulk) density adsorption layer with a distinctly non uniform coverage. The presence of the surface regions with low and non uniform water coverage suggests that the gas phase chemical oxidation mechanism may dominate in low density supercritical water. The tendency of supercritical water to favor ion association implies that the hydroxide/oxide layer would be relatively stable, and any further metal oxidation would occur by reaction with oxygen, in localized areas resulting in pitting corrosion. Supercritical water provides new and unique challenges [25] in the design of the SCWR and other technologies. More simulations with different substrate structures, over wider density ranges and with different gap spacing may provide a more comprehensive picture of its behavior in confined spaces and how it interacts with different materials.

Acknowledgements

This study has been conducted within the framework of the R&D activities of the Canadian National Program on Generation IV Energy Technologies. The authors are grateful for the financial support of the Atomic Energy of Canada Limited (AECL).

References

[1] M.D. Bermejo, M.J. Cocero, Supercritical water oxidation, American Institute of Chemical Engineering J. 52 (2006) 3933–3951.
[2] A. Kruse, E. Dinjus, Hot compressed water as a reaction medium and reactant: properties and synthesis reactions, J. Supercritical Fluids 39 (2007) 362–380.
[3] A. Kruse, H. Vogel, Heterogeneous catalysis in supercritical media: 2. Near critical and supercritical water, Chemical Engineering Technology 31 (2008) 1241–1245.
[4] P. MacDonald, J. Buongiorno, J.W. Sterbentz, C. Davis, R. Witt, Feasibility study of supercritical water cooled reactors for electric power production, in: Nuclear Energy Research Initiative Project, Idaho National Engineering and Environmental Laboratory, Bechtel BWXT Idaho, LLE, 2003.
[5] J. Kronholm, K. Hartonen, M.L. Riekkola, Analytical extractions with water at elevated temperatures and pressures, Trends in Analytical Chemistry 26 (2007) 396–412.
[6] F. Sanchez, L. Zhang, Interaction energies, structure and dynamics at functionalized graphitic structure–liquid phase interfaces in an aqueous calcium sulfate solution by molecular dynamics simulations, Carbon 48 (2010) 1210–1223.
[7] J. Wang, A.G. Kalinichev, R.J. Kirkpatrick, Molecular modeling of water structure in nano-pores between brucite (0 0 1) surfaces, Geochimica at Cosmochimica Acta 17 (2004) 3351–3365.
[8] C.D. Taylor, Atomistic modeling of corrosion events at the interface between a metal and its environment, International Journal of Corrosion 2012 (2012) 13.
[9] R.J. Kirkpatrick, A.G. Kalinichev, J. Wang, Molecular dynamics modeling of hydrated mineral interlayers and surfaces: structure and dynamics, Mineralogical Magazine 69 (2005) 287–306.
[10] S. Kerisit, J.H. Weare, A.R. Felmy, Structure and dynamics of fosterite–sc CO_2/H_2O interfaces as a function of water content, Geochimica et Cosmochimica Acta 84 (2012) 137–151.
[11] J. Bischoff, A.T. Motta, Oxidation behaviour of ferritic-martensitic and ODS steels in supercritical water, Journal of Nuclear Materials 424 (2012) 261–276.
[12] X. Luo, R. Tang, C. Long, Z. Maio, Q. Peng, C. Li, Corrosion behaviour of austenitic and ferritic steels in supercritical water, Nuclear Engineering and Technology 40 (2007) 147–154.
[13] G.S. Was, P. Ampornrat, G. Gupta, S. Teysseyre, E.A. West, Corrosion and stress corrosion cracking in supercritical water, Journal of Nuclear Materials 371 (2007) 176–201.
[14] P. Kritzer, Corrosion in high temperature and supercritical water and aqueous solutions: a review, Journal of Supercritical Fluids 29 (2004) 1–29.
[15] P. Kritzer, N. Boukis, E. Dinjus, The corrosion of alloy 625 ($NiCr_{22}Mo_9Nb$; 2.4856) in high temperature, high pressure aqueous solutions of phosphoric acid and oxygen, corrosion at sub and supercritical temperatures, Materials and Corrosion 49 (1998) 831–839.
[16] P. Kritzer, N. Boukis, E. Dinjus, Factors controlling corrosion in high temperature aqueous solutions: contributions to the dissociation and solubility data influencing corrosion processes, Journal of Supercritical Fluids 15 (1999) 205–227.
[17] C. Sun, R. Hui, W. Qu, S. Yick, Progress in corrosion resistant materials for supercritical water, Corrosion Science 51 (2009) 2508–2523.
[18] M.P. Allen, D.J. Tildesley, Computer Simulation of Liquids, Clarendon Press, NY, USA, 1989.
[19] A. Plugatyr, I.M. Svishchev, Accurate thermodynamic and dielectric equations of state for high temperature simulated water, Fluid Phase Equilibria 227 (2009) 145–151.
[20] A. Plugatyr, R. Carvajal-Ortiz, I.M. Svishchev, Ion-pair association constant for LiOH in supercritical water, Journal of Chemical and Engineering Data 56 (2011) 3637–3642.
[21] R.T. Cygan, J.J. Liang, A.G. Kalinichev, Molecular models of hydroxide, oxyhydroxide and clay phases and the development of a general force field, Journal of Physical Chemistry B 108 (2004) 1255–1266.
[22] R.T. Cygan, V.N. Romanov, E.M. Myshakin, Molecular simulation of carbon dioxide capture by montmorillonite using an accurate and flexible force field, Journal of Physical Chemistry 116 (2012) 13079–13091.
[23] R.S. Kavathekar, P. Dev, N.J. English, J.M.D. MacElroy, Molecular dynamics study of water in contact with the TiO_2 rutile-1 1 0, 1 0 0, 1 0 1, 0 0 1 and anatase-1 0 1, 0 0 1 surface, Molecular Physics 109 (2011) 1649–1656.
[24] D.A. Guzonas, W.G. Cook, Cycle chemistry and its effect on materials in a supercritical water-cooled reactor: a synthesis of current understanding, Corrosion Science 65 (2012) 48–66.
[25] I.M. Svishchev, D.A. Guzonas, Supercritical water and particle nucleation: implications for water chemistry control in a GEN IV supercritical water cooled nuclear reactor, Journal of Supercritical Fluids 60 (2011) 121–126.